Intravoxel Incoherent Motion Diffusion-Weighted MRI During Chemoradiation Therapy to Characterize and Monitor Treatment Response in Human Papillomavirus Head and Neck Squamous Cell Carcinoma

Ramesh Paudyal, PhD,[1] Jung Hun Oh, PhD,[1] Nadeem Riaz, MD,[2] Praveen Venigalla, MD,[2] Jingao Li, MD,[2,3] Vaios Hatzoglou, MD,[4] Jonathan Leeman, MD,[2] David Aramburu Nunez, MS,[1] Yonggang Lu, PhD,[5] Joseph O. Deasy, PhD,[1] Nancy Lee, MD,[2] and Amita Shukla-Dave, PhD[1,4]*

Purpose: Characterize and monitor treatment response in human papillomavirus (HPV) head and neck squamous cell carcinoma (HNSCC) using intra-treatment (intra-TX) imaging metrics derived from intravoxel incoherent motion (IVIM) diffusion-weighted magnetic resonance imaging (DW-MRI).
Materials and Methods: Thirty-four (30 HPV positive [+] and 4 HPV negative [-]) HNSCC patients underwent a total of 136 MRI including multi-b value DW-MRI (pretreatment [pre-TX] and intra-TX weeks 1, 2, and 3) at 3.0 Tesla. All patients were treated with chemo-radiation therapy. Monoexponential (yielding apparent diffusion coefficient [ADC]) and bi-exponential (yielding perfusion fraction [f], diffusion [D], and pseudo-diffusion [D*] coefficients) fits were performed on a region of interest and voxel-by-voxel basis, on metastatic neck nodes. Response was assessed using RECISTv1.1. The relative percentage change in D, f, and D* between the pre- and intra-TX weeks were used for hierarchical clustering. A Wilcoxon rank-sum test was performed to assess the difference in metrics within and between the complete response (CR) and non-CR groups.
Results: The delta (Δ) change in volume $(V)_{1wk\text{-}0wk}$ for the CR group differed significantly ($P = 0.016$) from the non-CR group, while not for $V_{2wk\text{-}0wk}$ and $V_{3wk\text{-}0wk}$ ($P > 0.05$). The mean increase in $\Delta D_{3wk\text{-}0wk}$ for the CR group was significantly higher ($P = 0.017$) than the non-CR group. ADC and D showed an increasing trend at each intra-TX week when compared with pre-TX in CR group ($P < 0.003$). Hierarchical clustering demonstrated the existence of clusters in HPV + patients.
Conclusion: After appropriate validation in a larger population, these IVIM imaging metrics may be useful for individualized treatment in HNSCC patients.
Level of Evidence: 2

J. MAGN. RESON. IMAGING 2017;45:1013–1023

Head and neck squamous cell carcinoma (HNSCC) was traditionally associated with behavioral risk factors, such as smoking and alcohol, but in the past decade, the human papillomavirus (HPV) infection has emerged as a novel etiologic agent of oropharyngeal carcinoma.[1] HPV negative (-) tumors continue to have poor prognosis despite

View this article online at wileyonlinelibrary.com. DOI: 10.1002/jmri.25523

Received Aug 12, 2016, Accepted for publication Oct 7, 2016.

*Address reprint requests to: A.S.-D., Department of Medical Physics and Radiology, Memorial Sloan Kettering Cancer Center, 1275 York Avenue, New York, New York 10065. E-mail: davea@mskcc.org

From the [1]Department of Medical Physics, Memorial Sloan Kettering Cancer Center, New York, New York, USA; [2]Radiation Oncology, Memorial Sloan Kettering Cancer Center, New York, New York, USA; [3]Department of Radiation Oncology, Jiangxi Cancer Hospital, Nanchang, P.R. China; [4]Department of Radiology, Memorial Sloan Kettering Cancer Center, New York, New York, USA; and [5]Department of Radiation Oncology, Washington University in St. Louis, St. Louis, Missouri, USA

treatment intensification.[2] In contrast, HPV-related tumors (HPV positive [+]) are associated with markedly improved outcomes and are now accepted as a distinct biological entity.[3,4] Marked improved prognosis in these patients has led to efforts that identify patients who may be candidates for treatment de-intensification, including dose de-escalation in radiotherapy.[3] Identifying patients with tumors exquisitely responsive to therapy would facilitate the next generation of clinical trials in HNSCC.

In vitro work with HPV + HNSCC cell line studies has suggested that radio-sensitivity of HPV + tumors is heterogeneous in nature, with some tumors appearing as resistant to radiation therapy as their HPV- counterparts.[5–7] Thus, careful patient selection is required for treatment with less aggressive radiotherapy regimens to maintain the excellent outcomes currently achieved with standard therapy.[3] In an era of personalized medicine, it is a prerequisite to better characterize HPV + and HPV- HNSCC before implementing a shift in the treatment paradigm.

The noninvasive diffusion-weighted MRI (DW-MRI) technique is sensitive to random thermal movement of water molecules and can probe the structure of biological tissues at the microscopic level.[8,9] Several reports have suggested that the quantitative imaging metric apparent diffusion coefficient (ADC), derived from DW-MRI data using a minimum of two b (b = diffusion-weighted gradient factor) values, has shown promise in clinical applications ranging from tumor characterization to the evaluation of treatment response.[10–12] It has been reported that hypercellular tissue is characterized by low ADC, whereas hypocellular tissue with necrosis, or apoptosis, is characterized by high ADC; the change in ADC (ΔADC) before, during, or after chemoradiation therapy in HNSCC is a surrogate biomarker of treatment response.[13,14]

Furthermore, multi-b value DW-MRI data allows for fitting the data using the intravoxel incoherent motion (IVIM) model, which measures both Brownian water molecular diffusion and blood perfusion in the capillary network.[15] The quantitative imaging metrics, derived from IVIM, are the diffusion coefficient (D), perfusion fraction (f) and pseudo-diffusion coefficient (D*), measured without the use of a contrast agent.[16,17] Recently, feasibility studies have shown the utility of IVIM DW-MRI in the characterization of HNSCC.[18–21]

Although DW-MRI has shown promise in the assessment of treatment response, its role in facilitating the recognition of sub-entities within HPV tumors that are exquisitely sensitive to radiation therapy remains unexplored. The present study aims to characterize and monitor treatment response in HPV HNSCC using intra- treatment (TX) imaging metrics derived from IVIM DW-MRI. Inspired by an idea used in many studies that have used clustering approaches for finding sub-entities in cancer.[22–24] In this study, we will use an unsupervised hierarchical clustering with a distance measure based on the Pearson correlation coefficient to investigate similarities among features and samples.

Materials and Methods

Study Design

Our institutional review board approved this prospective study that is compliant with the Health Insurance Portability and Accountability Act. We obtained written informed consent from all eligible patients who have had biopsy-proven, newly diagnosed HNSCC; diagnostic biopsies were tested for HPV status before the MRI study. Between December 2013 and November 2015, a total of 40 HPV patients were enrolled into the study. Six of these patients were then removed from the study; two of the patients did not have intra-TX data and four patients were excluded due to image distortions resulting from motion and susceptibility artifacts. A total of 34 HPV (30 HPV + and 4 HPV−) HNSCC patients (age, 30–82 years; male, 31; female, 3) were included in this study. Among these patients, eight had bilateral metastatic neck nodes. Patient characteristics are given in Table 1. A total of 136 MRI studies were performed (Fig. 1) with anatomic and DW-MRI sequences (pre-TX, weeks 1, 2, and 3 intra-TX). Patients were treated with chemotherapy and radiotherapy (70 Gy). The treatment details are summarized in Table 2. Response Evaluation Criteria in Solid Tumors (RECIST) 1.1 guidelines[25] were used to categorize patients into groups (i.e., progressive disease [PD], stable disease [SD], partial response [PR], or complete response [CR]) based on the ^{18}F-fluorodeoxyglucose (^{18}F-FDG) positron emission tomography/computed tomography (PET)/CT, performed 3–6 months after treatment completion.

MR Imaging Data Acquisition

MRI examinations were performed on a Philips 3 Tesla (T) MRI scanner (Ingenia; Philips Healthcare, Netherlands) using a neurovascular phased-array coil (maximum number of channels: 20). The standard MR acquisition parameters were as follows: multiplanar (axial, coronal, and sagittal) T_2-weighted (T_{2W}), fat-suppressed, fast spin-echo images (repetition time [TR] = 4000 ms; echo time [TE] = 80 ms; number of averages (NA) = 2; matrix = 256 × 256; slice thickness = 5 mm; field of view [FOV] = 20–24 cm), and multiplanar T_1-weighted (T_{1W}) images (TR = 600 ms; TE = 8 ms; NA = 2; slice thickness = 5 mm; matrix = 256 × 256; FOV = 20–24 cm). Standard T_1w and T_{2w} imaging was followed by DW-MRI.

The DW-MRI data were acquired using a single-shot echo planar imaging (SS-EPI) sequence with 10 b-values (i.e., b = 0, 20, 50, 80, 200, 300, 500, 800, 1500, and 2000 s/mm^2) in a single MR acquisition scan. Other MR parameters were as follows: TR = 4000 ms, TE (shortest [minimum]) fixed in a single scan, NA = 2, matrix = 128 × 128, FOV = 20–24 cm, slices = 8–10, slice thickness = 5 mm. The total acquisition time for the multi b-value data acquisition was approximately 5 min. The acquisition TE varied between patients (TE range, 80–100 ms), because of slight differences in obliquity of the prescription. The total acquisition time was approximately 30 min for the whole examination.

TABLE 1. Patient Characteristics

Characteristics	CR (n, %)	non-CR (n, %)
Age (years)		
Median	57	56
Range	30-82	51-61
Sex		
Male	28 (93%)	3 (75%)
Female	2 (7%)	1 (25%)
KPS		
Median	90	90
Range	70-100	80-90
Alcohol consumption		
Yes	25 (83%)	3 (75%)
No	5 (17%)	1 (25%)
Tobacco history		
Yes	17 (57%)	3 (75%)
No	13 (43%)	1 (25%)
Clinical stage		
III	1 (3%)	1 (25%)
Vla	29 (97%)	3 (75%)
Primary tumor location		
Oropharynx	28 (93%)	4 (100%)
Unknown primary	2 (7%)	0
HPV Status		
Positive	27 (90%)	3 (75%)
Negative	3 (10%)	1 (25%)

TABLE 2. Treatment Details of Chemoradiation for the HNSCC Patients

Radiation dose (Gy)	CR (n, %)	non-CR (n, %)
Median	70	70
Chemotherapy		
Yes	30 (100%)	3 (75%)
No	0	1 (25%)
Chemotherapy regimen		
Cisplatin	25 (79%)	2 (67%)
Cetuximab	2 (9%)	0
Carboplatin/5-FU	3 (12%)	1 (33%)

Multi-b Value DW-MRI Image Analysis

The multi b-value DW-MRI data were fitted to the models detailed below: (a) monoexponential model[8] (Eq. [1]) was used to calculate ADC (mm^2/s) with all the b-values,

$$S_1 = S_0 \ exp(-bADC) \tag{1}$$

and (b) bi-exponential IVIM model (15) (Eq. [2]) as

$$S_2 = S_0 \ [(1-f)exp(-bD) + fexp(-bD^*)] \tag{2}$$

where S_0 is the signal intensity without diffusion weighting, S_1 and S_2 represent the signal intensity with the diffusion weighting gradient factor, b (s/mm^2). Also, f is the perfusion fraction, D is the diffusion coefficient (mm^2/s), and D* is the pseudo-diffusion coefficient (mm^2/s).

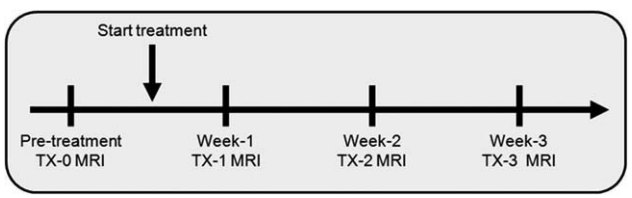

FIGURE 1: Timeline illustrating the consecutive MRI examinations.

The imaging metrics derived from IVIM DW-MRI were estimated using a nonlinear least-square curve fitting method as detailed by Lu et al.[20,26] All postprocessing analyses were performed using in-house scripts written in MATLAB (Mathworks, Natick, MA).

Finally, a relative (r) percentage change in imaging metrics between pre- and i^{th} intra-TX week with pre-TX was calculated as:

$$rW_{iwk-0wk}(\%) = \frac{(W_{iwk} - W_{0wk})}{W_{0wk}} \times 100 \tag{3}$$

where W_{0wk} and W_{iwk} represent the pre- and ith intra-TX week (i.e., i = 1, 2 and 3) for ADC, f, D, D* and total tumor volume, respectively.

Before contouring the regions of interest (ROIs), the T_{2w}/T_{1w} images were used as references to determine tumor extent. All diffusion-weighted images were registered to the b = 0 [s/mm^2] image. ROIs were delineated on the neck nodal metastases by a team of radiation oncologist (N.R., > 5 years of imaging experience) and a neuroradiologist (V.H., > 10 years of imaging experience), on the IVIM DW-MRI image (b = 0 s/mm^2) with the Eclipse treatment planning system (Varian Medical Systems, Palo Alto, CA, USA). ROIs were imported by means of an in-house script written in MATLAB for image analysis. For each patient, the total tumor volume was calculated by summing the volume for all slices that contained tumor tissue on T_{2w} images using ImageJ.[27] The ROIs were fitted on a voxel-by-voxel basis for parametric maps and histograms.

Statistical Analysis

In the present study, the pre-TX and first, second, and third weekly intra-TX ADC, IVIM diffusion metrics (f, D, and D*), and the total tumor volumes were used to capture early treatment-related changes. The imaging metrics for the ROIs were averaged to yield the mean and the standard deviation (SD). To examine which HPV HNSCC patients may cluster together, a heat map with unsupervised hierarchical clustering was generated using IVIM imaging metrics of the relative percentage changes observed in the

TABLE 3. Pre- and Intra-TX IVIM DW-MRI Derived Metric Values for HNSCC Patients[a]

Treatment assessment	ADC×10^{-3} (mm^2/s)				D×10^{-3} (mm^2/s)				D*×10^{-3} (mm^2/s)				f			
	Pre-TX wk0	Intra-TX wk1	Intra-TX wk2	Intra-TX wk3	Pre-TX wk0	Intra-TX wk1	Intra-TX wk2	Intra-TX wk3	Pre-TX wk0	Intra-TX wk1	Intra-TX wk2	Intra-TX wk3	Pre-TX wk0	Intra-TX wk1	Intra-TX wk2	Intra-TX Wk3
CR (n = 30)	0.94 ± 0.21	1.06 ± 0.25	1.23 ± 0.30	1.28 ± 0.29	0.67 ± 0.17	0.79 ± 0.21	0.96 ± 0.29	0.98 ± 0.28	9.71 ± 2.29	9.44 ± 2.68	8.94 ± 2.88	9.32 ± 3.11	0.16 ± 0.04	0.15 ± 0.04	0.14 ± 0.05	0.14 ± 0.06
Non-CR (n = 4)	0.82 ± 0.07	0.92 ± 0.05	1.03 ± 0.09	1.02 ± 0.12	0.59 ± 0.10	0.67 ± 0.08	0.75 ± 0.10	0.72 ± 0.03	7.86 ± 1.57	11.02 ± 2.80	11.00 ± 1.43	9.69 ± 2.76	0.16 ± 0.03	0.13 ± 0.04	0.15 ± 0.03	0.15 ± 0.06

[a]The data are mean ± SD.

first, second and third weekly intra-TX values for D, f and D*. This resulted in a total of nine sets of values for the relative percentage change of the three imaging metrics. The hierarchical clustering was performed with a distance measure based on the Pearson correlation coefficient using an R software package *gplots*,[28] which is an unsupervised analysis as it does not consider the outcomes (CR or non-CR) in the analysis. As a note, the goal of this analysis is to group those samples that are close distance to one another with the hypothesis that one of the clusters may include patients with worse outcomes (non-CR, in this study), not to find the optimal number of clusters. Also, the non-CR group consisted of PD, SD, and PR patients.

A nonparametric Wilcoxon rank sum test (WRST) was performed to assess the differences in the imaging metric values within and between CR and non-CR groups during treatment weeks. Bonferroni correction was applied to address the multiple comparisons between the intra-TX and pre-TX (i.e., 5 metrics: ADC, f, D, D* and total tumor volume at three time points). A P-value < 0.05 was considered statistically significant (before correction for multiple comparisons) and an adjusted P-value < 0.003 (0.05/15) was regarded as statistically significant after Bonferroni correction. The results are presented with and without Bonferroni correction. All data analyses were performed using the Stata[29] and R software.[28]

Results

In total, 136 MRI exams from 34 HNSCC patients were successfully performed using the multi-b value DW-MRI acquisition protocol. The CR group patients median age was 57 years (range, 30–82 years; 28 male and 2 female) whereas non-CR group patients median age was 56 years (range: 51–61 years, 3 male and 1 female). The medians Karnofsky Performance Status (KPS) for CR and non-CR group patients were 90 (range, 70–100) and 90 (range, 80–90) (Table 1). Of 34 patients, 30 were classified into the CR group (27 HPV + and 3 HPV-) and 4 into the non-CR group (3 HPV + and 1 HPV-), based on the ^{18}F-FDG PET/CT performed 3–6 months after treatment completion. In the non-CR group, HPV + consisted of two PR patients and one SD patient; HPV- consisted of one PR patient.

Within the CR group, the mean total tumor volume at intra-TX week 3 was significantly different ($P < 0.05$ (WRST); $P < 0.003$ after Bonferroni correction) from that of pre-TX, i.e., volume reduction of 58%. In the non-CR group, there was only a substantial reduction (44%; $P > 0.05$) in mean total tumor volumes between intra-TX week 3 and pre-TX. The mean delta(Δ) change in volume $(V)_{1wk\text{-}0wk}$ in the CR was significantly higher than in the non-CR group ($P = 0.016$ [WRST], noting that the adjusted P value was not considered statistically significant after Bonferroni correction). Also, $\Delta V_{2wk\text{-}0wk}$ and $\Delta V_{3wk\text{-}0wk}$ values were not significantly different between CR and non-CR groups ($P > 0.05$). Table 3 shows the mean ± SD for the metrics ADC, D, f and D* at each imaging time point for HNSCC patients. The adjusted P values obtained by means of Bonferroni correction were reported for multiple

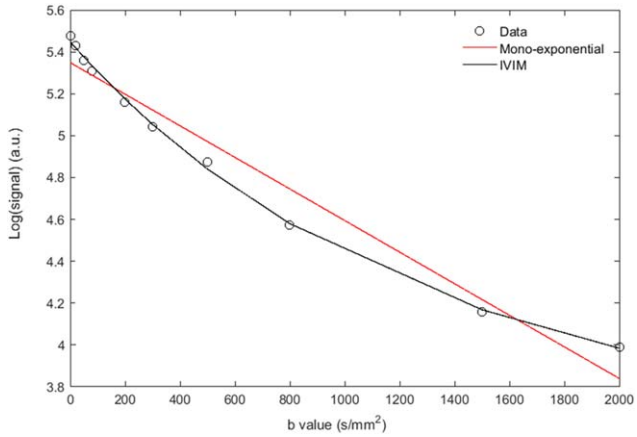

FIGURE 2: An example of mean semilogarithmic signal intensity decay curve as a function of the b-value obtained from the metastatic neck node of a patient who experienced CR. The open circle represents the experimental data, and the red and black solid lines are the fitted curves for the monoexpeontial model and IVIM based analysis.

comparisons. The mean pre-TX ADC, D, f, and D* values in the CR group did not differ significantly from those in the non-CR group ($P > 0.003$ for all).

In summary, for the CR group, ADC and D showed a statistically significant increasing trend at each intra-TX week when compared with pre-TX ($P < 0.003$ for all). Also, the mean f values at intra-TX weeks 2 and 3 tend to be lower than those at the pre-TX week ($P > 0.003$ for both intra-TX week 2 and week 3). On the other hand, D* did not show a trend toward significance at any intra-TX week when compared with pre-TX ($P > 0.003$ for all). While for the non-CR group, ADC and D values showed an increasing trend at each intra-TX week when compared with pre-TX, but were not statistically significant ($P > 0.003$ for all). Also, f and D* did not show any trend toward significance at any intra-TX week when compared with pre-TX ($P > 0.003$ for all). At intra- TX week 3, the mean ADC and D values in the CR group tend to be higher than those in the non-CR group ($P > 0.003$ for ADC and D). Also, the change in CR group f between intra-TX week 3 and pre-TX ($\Delta f_{3wk\text{-}0wk}$) showed a trend when compared with the non-CR group ($P > 0.003$).

Figure 2 shows an example of mean semilogarithmic signal intensity decay curve as a function of the b-value

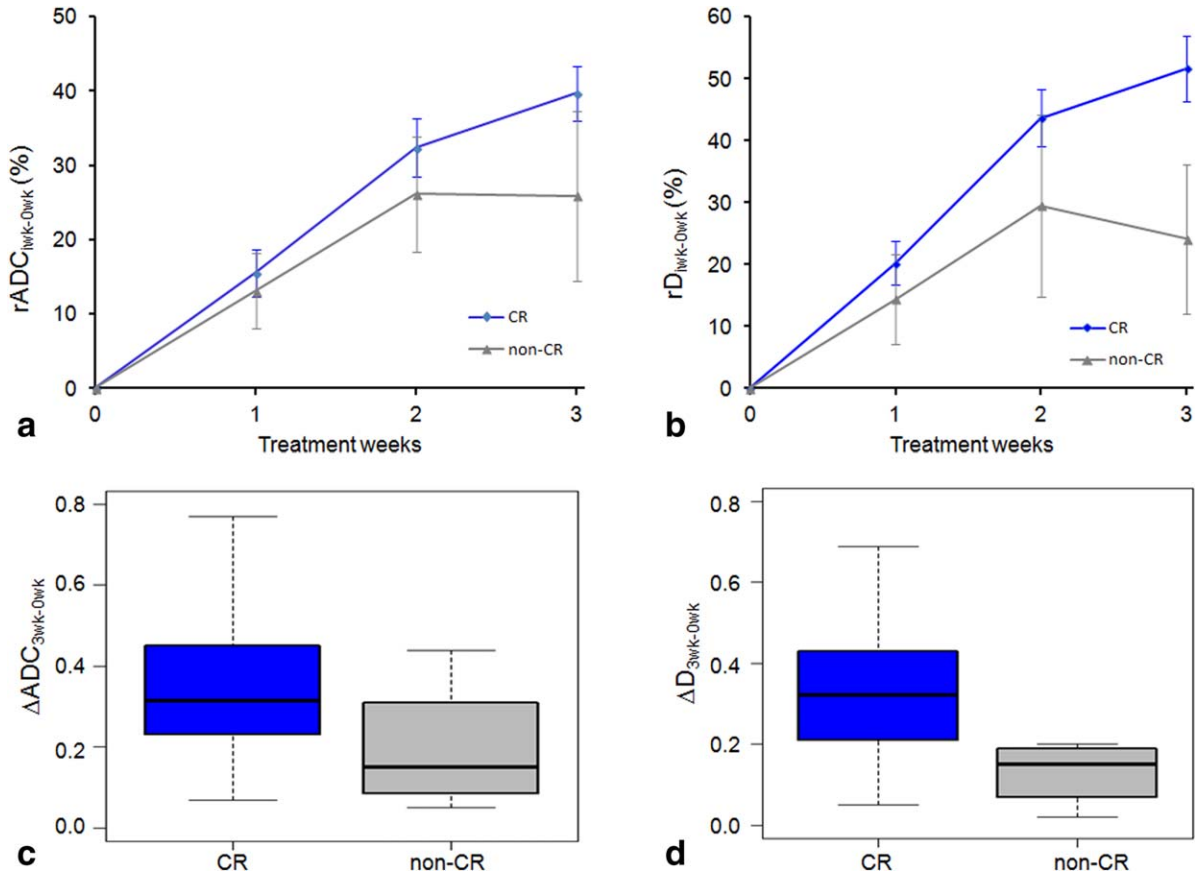

FIGURE 3: A line graph of the mean $rADC_{iwk\text{-}0wk}$ (%) (a) and $rD_{iwk\text{-}0wk}$ (%) (b) during treatment weeks for the CR and non-CR groups. Error bars represent the standard error of the mean. $rD_{3wk\text{-}0wk}$ was significantly higher in CR group compared with non-CR group ($P = 0.007$), whereas $rADC_{3wk\text{-}0wk}$ did not show significant ($P > 0.05$). Box plots comparing $\Delta ADC_{3wk\text{-}0wk} \times 10^{-3}$ (mm^2/s) (c) and $\Delta D_{3wk\text{-}0wk} \times 10^{-3}$ (mm^2/s) (d) for patients showing CR and non-CR. $\delta D_{3wk\text{-}0wk}$ was significantly higher for patients showing CR as compared with non-CR ($P = 0.017$), whereas $\Delta ADC_{3wk\text{-}0wk}$ did not show significant ($P > 0.05$). The bottom and top of the boxes indicate 25th and 75th percentiles of the values, respectively. The horizontal line inside the box indicates median values. *P*-values were computed using a Wilcoxon rank sum test to compare the metric values between the CR and non-CR groups.

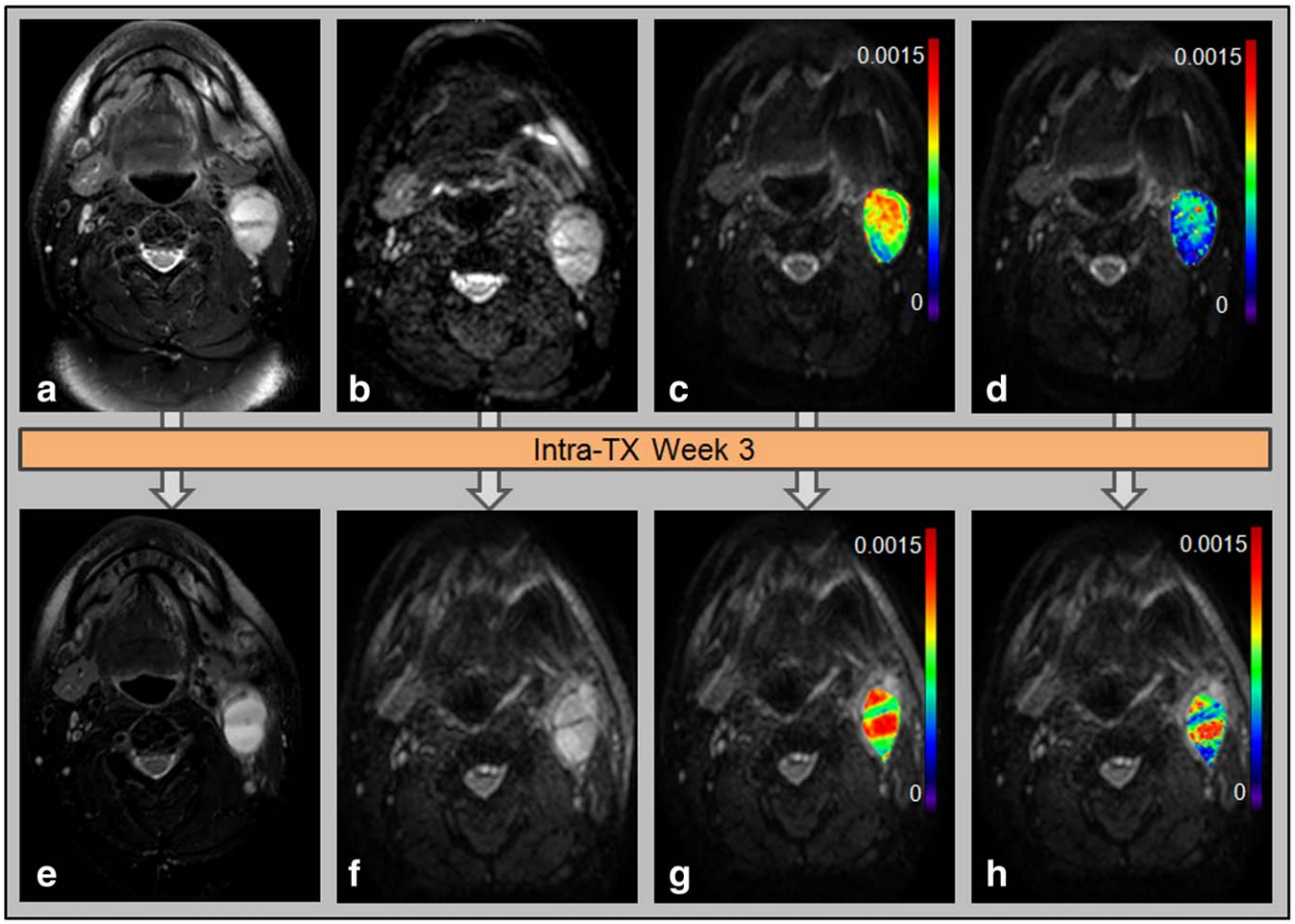

FIGURE 4: Representative pre-TX (top) and intra-TX week 3 (bottom) MR images of a patient who showed CR (52 years, male). T2-weighted images (a,e). Diffusion-weighted (b = 0 s/mm^2) images (b,f). ADC (mm^2/s) (c,g) and D (mm^2/s) (d,h) map overlaid on DW (b = 0 s/mm^2) images.

obtained from the metastatic neck node of a patient who experienced CR. The data were fitted to both monoexponential and the IVIM models. It can be clearly appreciated that IVIM based analysis fits the data points substantially better ($R^2 = 0.99$) than the monoexponential model ($R^2 = 0.96$) for an extended b value range of up to 2000 s/mm^2.

Figure 3a,b demonstrates the mean relative percentage changes (mean ± SD) in ADC ($rADC_{iwk\text{-}0wk}$) and D ($rD_{iwk\text{-}0wk}$), respectively, during the 3 treatment weeks for the CR and non-CR groups. The $rADC_{3wk\text{-}0wk}$ and $rD_{3wk\text{-}0wk}$ reached a percentage increase of 40 ± 20.% and 52 ± 29% for the CR group, respectively, whereas for the non-CR group these values were 26 ± 23% and 24.0 ± 16%, respectively. At the intra-TX week 3, the mean $rD_{3wk\text{-}0wk}$ value in the CR group tends to be higher than in the non-CR group ($P = 0.007$ (WRST), but not significant after Bonferroni correction), whereas $rADC_{3wk\text{-}0wk}$ did not show significant ($P > 0.05$). Error bars represent the standard error of the mean.

Figure 3c,d shows box and whisker plots comparing the changes in imaging metric values between intra-TX week 3 and pre-TX ($\Delta ADC_{3wk\text{-}0wk}$ and $\Delta D_{3wk\text{-}0wk}$) for the CR and non-CR groups. For the CR group, $\Delta D_{3wk\text{-}0wk}$ was significantly higher than the non-CR group ($P = 0.017$ (WRST), noting that the adjusted P value was not considered statistically significant after Bonferroni correction). $\Delta ADC_{3wk\text{-}0wk}$ in the CR group showed a trend toward higher value than in the non-CR group ($P = 0.06$ [WRST]).

Figure 4 illustrates MR images, pre- and intra-TX week 3, with overlaid parametric maps from a patient (52 years, male) who showed CR (HPV+). Similarly, Figure 5 shows MR images, pre- and intra-TX week 3, with overlaid parametric maps from a patient (51 years, female) who showed non-CR (HPV-).

Figure 6a,b shows the histogram distributions of the pre- and intra-TX week 3 measures of ADC and D, within the ROIs of the metastatic neck node, for the same CR and non-CR patients. A shift of ADC and D values toward a higher value at intra-TX week 3 in CR group can be clearly seen, whereas in the non-CR group no major changes in ADC and D values were observed.

Figure 7 shows a heat map generated from the unsupervised hierarchical clustering analysis using a total of nine set of values for all 34 patients. After the generation of the

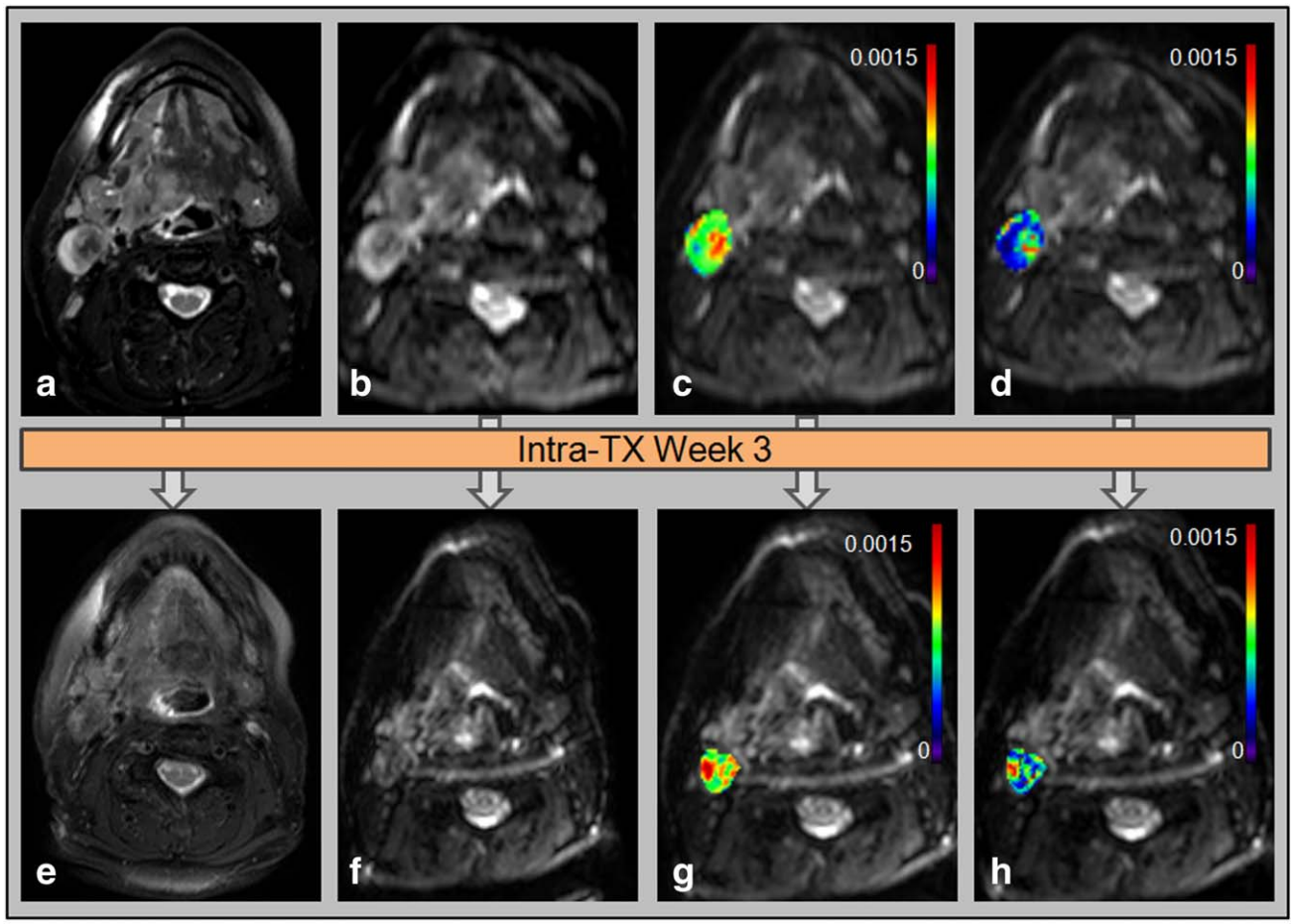

FIGURE 5: Representative pre-TX (top) and intra-TX week 3 (bottom) MR images of a patient who showed non-CR (51 years, female). a,e: T2-weighted images. b,f: Diffusion-weighted (b = 0 s/mm^2) images. ADC (mm^2/s) (c,g) and D (mm^2/s) (d,h) maps overlaid on DW (b = 0 s/mm^2) images.

heat map, we marked HPV status (blue and red color bar) and clinical response status (the red circles on the right side indicate non-CR patients) on it. It is interesting to note that in the top big cluster consisting of 13 patients, 3 of 4 HPV- patients were clustered together and all 4 non-CR patients belonged to the same cluster, indicating the possibility of the existence of subtypes in HPV + HNSCC patients.

Discussion

In this study, we investigated the utility of IVIM DW-MRI for early assessment of treatment response to chemo-radiation therapy in HNSCC patients. The CR group demonstrated linear increasing trends for the relative mean percentage change in ADC and D values within the treatment weeks. This was not observed in the non-CR group where these values increased at the early phase of treatment, but decreased at intra-TX week 3. Our initial results suggest that intra-TX week 3 may be a critical time point for early response monitoring in HPV + HNSCC patients. An early increase in ADC, and/or D, may reflect changes in tumor cellularity and cell membrane integrity due to apoptosis and necrosis during chemo-radiation. The ADC incorporates the effects of both perfusion and diffusion, whereas D is associated to molecular diffusion. Our findings regarding the D and f values are consistent with previous studies.[18,19] Kim et al found that the median nodal tumor volume of the PR group was higher, but not significantly different from that of the CR group.[11] In addition, the median volumes decreased significantly in the CR group at weeks 1 and post-TX compared with the volumes at pre-TX.[11] In our study, the CR group demonstrated similar results with a significant reduction in the total tumor volume during the therapy.

Previous studies have reported that changes in water diffusivity, affected by tumor cellularity, enable predictive response of metastatic tumors to therapeutic interventions.[11,30,31] A recent study used ADC as a marker to compare the mean pretreatment ADC values between HPV + (n = 6) and HPV- (n = 67) HNSCC and found that HPV + HNSCC showed significantly lower ADC compared with HPV-.[32] In HNSCC, cellular tumors with lower pre-TX ADC values have shown a more favorable outcome to chemo-radiation therapy than necrotic tumors with higher pre-TX ADC values.[12,33]

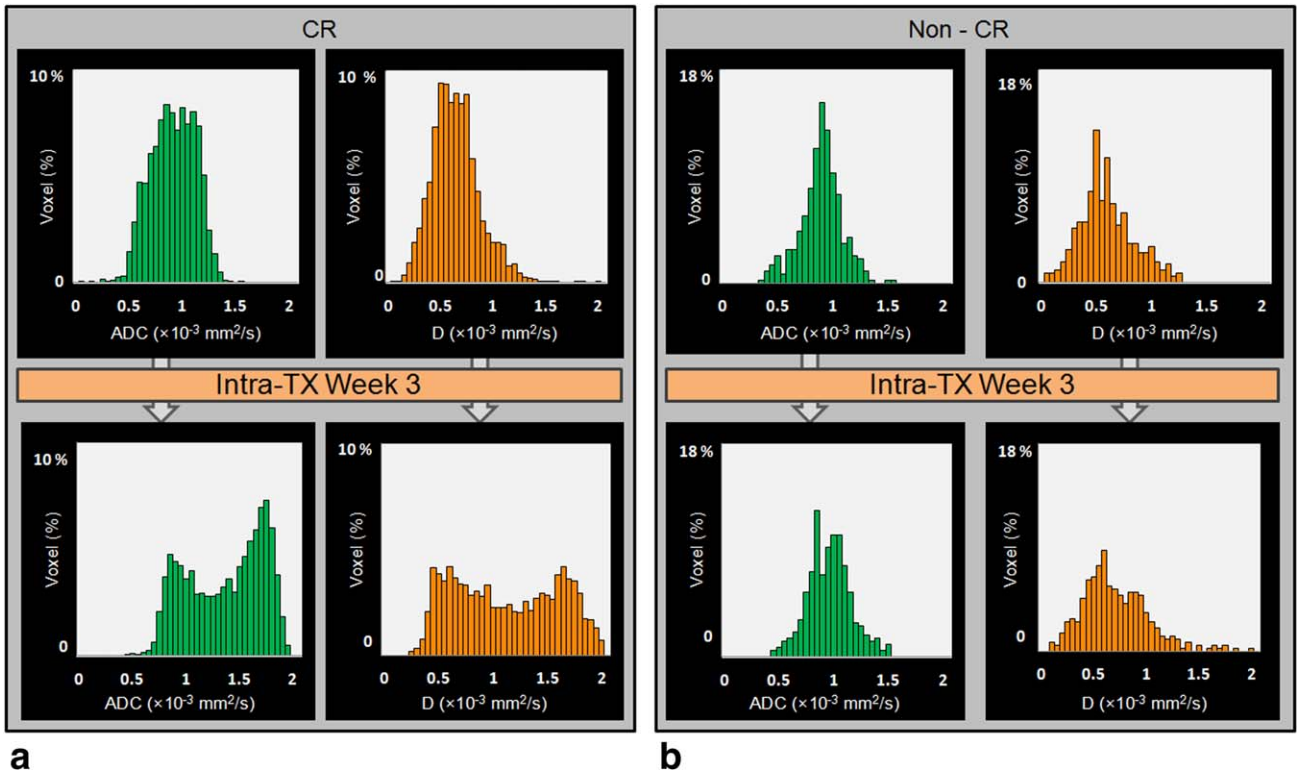

FIGURE 6: a,b: The histogram distributions of the pre- and intra-TX week 3 measures of ADC and D, within the ROIs of the metastatic neck node, for the same CR and non-CR patients. Histograms represent the voxel distribution (%) of pre- and intra-TX week3 ADC and D in the CR and non-CR groups.

Vandecaveye et al[14] reported that ΔADC in primary tumors and nodal metastases, 2 and 4 weeks after the start of chemo-radiation therapy, were significantly lower in lesions with post-TX recurrence than in lesions with CR for primary tumors, relative to nodal metastases. Also, King et al[13] reported a significant correlation between local failure and post-TX ADC, but not pre- or intra-TX ADC values. Kim et al[11] reported a significant increase in ADC values observed in the CR group within 1 week of treatment in HNSCC. Our results also showed an increase in ADC values in the CR group at the intra-TX week 3 compared with the non-CR group.

The ADC and/or D histogram(s) display(s) functional differences in tumor tissue due to the microstructural heterogeneity as seen in a previous study.[34] Thus, the distribution of tumor ADC values represented by a histogram may be important in assessing tumor response in HNSCC. Srinivasan et al[35] showed that ADC histograms were able to depict the heterogeneity of a lesion (viable portions showed lower ADC values than those of the necrotic portions) in HNSCC. In the CR group of our study, ADC and D histograms in intra-TX week 3 had shifted toward the right when compared with pre-TX, indicating an increase in mean ADC and D values, whereas in the non-CR group, ADC and D histograms showed less of a shift to the right side because of a smaller increase in the mean ADC and D values. A shift toward a higher ADC and/or D value(s) reflect(s) the improved response to chemo-radiation therapy.

IVIM-derived metrics, including D, D*, and f are unique as they are able to assess diffusion and perfusion in a tumor without the use of a contrast agent.[16,17] Hauser et al reported in a 15 patient feasibility study that pre-TX D values were not significantly different, while f was significantly higher in patients with local regional failure compared with those with local regional control.[19] While Ding et al recently reported in an IVIM DW-MRI study with 31 HNSCC patients that mid-TX values for ADC, D, and f were significantly higher than the pre-TX values for all lesions.[18] In our study, D values at intra-TX week 3 increased significantly in the CR group compared with the non-CR group. Furthermore, $\Delta D_{3wk\text{-}0wk}$ also demonstrated the statistically significant difference between the CR and non-CR groups, whereas $\Delta f_{3wk\text{-}0wk}$ showed a trend toward higher value in the CR group with non-CR group. This indicated that ΔD and Δf can be useful metrics to noninvasively assess diffusion and perfusion fraction without a contrast agent for assessment of treatment response in HNSCC patients. These metrics may also be useful to identify HPV + patients eligible for potential dose de-escalation in future studies. The reproducibility of the IVIM techniques was not assessed in this study, although, the reproducibility of the IVIM technique has been previously investigated and

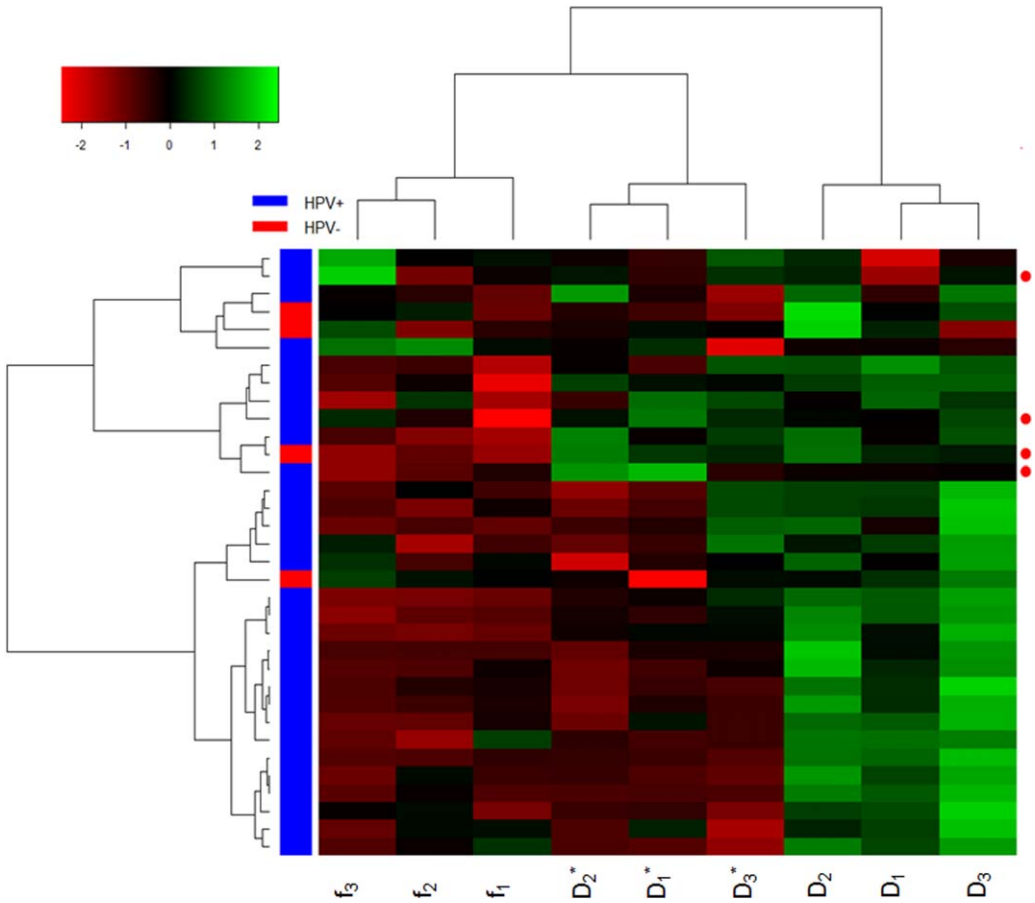

FIGURE 7: Clustering results. Heat map from hierarchical clustering. The red circles on the right indicate patients with non-CR. The $f_{(1, 2, 3)}$, $D_{(1, 2, 3)}$ and $D^*_{(1, 2, 3)}$ represent the relative percentage change of f, D, and D* in weeks 1, 2, and 3, respectively.

found high reproducibility for D with compared to f and D*.[36] So far, f and D* remain exploratory in nature as the biological meaning for these metrics has yet to be fully explored and understood.

To capture the basic heterogeneity in the tumor biology of HPV+/- HNSCC with IVIM DW-MRI metrics, we used a hierarchical clustering that provides quantitative and visual stability evidence in estimating the possibility of the existence of clusters in a specific group. This unsupervised clustering method does not identify the most significant imaging metric that could be driving the cluster formation, but instead uses all the IVIM DW-MRI imaging metric values without prior knowledge. The hypothesis in this study is that in the identified clusters we may observe that patients with worse outcomes (non-CR) are grouped. Considering this, we chose to use a hierarchical clustering. Compared with K-means clustering, an advantage of using hierarchical clustering is that the number of clusters is not required as an input. This clustering approach was successful in identifying the possibility of the existence of clusters in the HPV + HNSCC group and it highlights the importance of imaging at early time points during therapy. Our initial report lays the building block for larger population validation studies that would enable physicians to re-evaluate patients at week 3 during treatment thereby optimizing individual dose treatment plans while minimizing toxicities for a sub-entity of HPV + HNSCC patients.

In this preliminary pilot study of 34 HPV+/− HNSCC patients we analyzed data from 136 MRI exams. As a note, the non-CR group has a small sample size (n = 4), allowing only basic comparisons between the CR and non-CR groups during treatments. However, clinical validation, based on a larger patient sample size, is warranted in future studies. The signal-to-noise ratio (SNR) for images acquired with higher b-values, in multi b-value DW-MRI acquisition, is lower compared with the SNR in low b-value images. Voluntary and involuntary bulk motion, or severe susceptibility artifacts due to SS-EPI, is still an issue in the head and neck region. In the future, sequences, such as reduced field of view SS-EPI, would help acquire images with reduced distortions. Finally, the exact nature of the IVIM DW-MRI model needs to be further elucidated.

Using IVIM DW-MRI imaging metrics in hierarchical clustering, the present feasibility study shows interesting initial results and suggests that there may be sub-entities in HPV + HNSCC patients undergoing chemoradiation therapy. In the future, these IVIM DW-MRI imaging metrics, obtained pre-TX and early during TX (weekly until the 3rd

week), can help identify patients who may benefit from dose de-escalation and reduced toxicity based on the inherent biology of the specific tumor.

In summary, $\Delta V_{1w\text{-}0wk}$ and $\Delta D_{3w\text{-}0wk}$ were significantly different between the CR and non-CR groups. A hierarchical clustering approach, shown on a heat map, using IVIM DW-MRI, identified sub-entities in HPV + HNSCC patients. This emphasizes the heterogeneity in the radiosensitivity of these tumors. These results are preliminary in nature and are indicative, and not definitive, trends portrayed in HNSCC patients with nodal disease. After appropriate validation in a larger HNSCC population, these findings may be useful in individualized patient care.

Acknowledgments

Contract grant sponsor: MSKCC internal IMRAS grant; Contract grant sponsor: NIH/NCI Cancer Center Support Grant; contract grant number: P30 CA008748

The authors thank the MRI technologists for their great efforts in helping to perform the MRI examinations and Mr. Christian Czmielewski for his helpful contribution to patient enrollment and data management. We thank Mr. James Keller for editing the manuscript. The authors have no conflicts of interest to disclose.

References

1. Psyrri A, Rampias T, Vermorken JB. The current and future impact of human papillomavirus on treatment of squamous cell carcinoma of the head and neck. Ann Oncol 2014;25:2101–2115.
2. Leemans CR, Braakhuis BJM, Brakenhoff RH. The molecular biology of head and neck cancer. Nat Rev Cancer 2011;11:9–22.
3. O'Sullivan B, Huang SH, Siu LL, et al. Deintensification candidate subgroups in human papillomavirus-related oropharyngeal cancer according to minimal risk of distant metastasis. J Clin Oncol 2013; 31:543–550.
4. Huang SH, Perez-Ordonez B, Weinreb I, et al. Natural course of distant metastases following radiotherapy or chemoradiotherapy in HPV-related oropharyngeal cancer. Oral Oncol 2013;49:79–85.
5. Kimple RJ, Smith MA, Blitzer GC, et al. Enhanced radiation sensitivity in HPV-positive head and neck cancer. Cancer Res 2013;73:4791–4800.
6. Park JW, Nickel KP, Torres AD, Lee D, Lambert PF, Kimple RJ. Human papillomavirus type 16 E7 oncoprotein causes a delay in repair of DNA damage. Radiother Oncol 2014;113:337–344.
7. Rieckmann T, Tribius S, Grob TJ, et al. HNSCC cell lines positive for HPV and p16 possess higher cellular radiosensitivity due to an impaired DSB repair capacity. Radiother Oncol 2013;107:242–246.
8. Chenevert TL, Ross BD. Diffusion imaging for therapy response assessment of brain tumor. Neuroimaging Clin N Am 2009;19: 559–571.
9. Padhani AR, Koh DM. Diffusion MR imaging for monitoring of treatment response. Magn Reson Imaging Clin N Am 2011;19:181–209.
10. Jansen JF, Koutcher JA, Shukla-Dave A. Non-invasive imaging of angiogenesis in head and neck squamous cell carcinoma. Angiogenesis 2010;13:149–160.
11. Kim S, Loevner L, Quon H, et al. Diffusion-weighted magnetic resonance imaging for predicting and detecting early response to chemoradiation therapy of squamous cell carcinomas of the head and neck. Clin Cancer Res 2009;15:986–994.
12. Vandecaveye V, Dirix P, De Keyzer F, et al. Diffusion-weighted magnetic resonance imaging early after chemoradiotherapy to monitor treatment response in head-and-neck squamous cell carcinoma. Int J Radiat Oncol Biol Phys 2012;82:1098–1107.
13. King AD, Mo FK, Yu KH, et al. Squamous cell carcinoma of the head and neck: diffusion-weighted MR imaging for prediction and monitoring of treatment response. Eur Radiol 2010;20:2213–2220.
14. Vandecaveye V, Dirix P, De Keyzer F, et al. Predictive value of diffusion-weighted magnetic resonance imaging during chemoradiotherapy for head and neck squamous cell carcinoma. Eur Radiol 2010; 20:1703–1714.
15. Le Bihan D, Breton E, Lallemand D, Grenier P, Cabanis E, Laval-Jeantet M. MR imaging of intravoxel incoherent motions: application to diffusion and perfusion in neurologic disorders. Radiology 1986; 161:401–407.
16. Le Bihan D. Intravoxel incoherent motion imaging using steady-state free precession. Magn Reson Med 1988;7:346–351.
17. Le Bihan D, Turner R, Douek P, Patronas N. Diffusion MR imaging: clinical applications. AJR Am J Roentgenol 1992;159:591–599.
18. Ding Y, Hazle JD, Mohamed AS, et al. Intravoxel incoherent motion imaging kinetics during chemoradiotherapy for human papillomavirus-associated squamous cell carcinoma of the oropharynx: preliminary results from a prospective pilot study. NMR Biomed 2015;28:1645–1654.
19. Hauser T, Essig M, Jensen A, et al. Prediction of treatment response in head and neck carcinomas using IVIM-DWI: evaluation of lymph node metastasis. Eur J Radiol 2014;83:783–787.
20. Lu YG, Jansen JFA, Stambuk HE, et al. Comparing primary tumors and metastatic nodes in head and neck cancer using intravoxel incoherent motion imaging: a preliminary experience. J Comput Assist Tomogr 2013;37:346–352.
21. Xiao-Ping Y, Jing H, Fei-Ping L, et al. Intravoxel incoherent motion MRI for predicting early response to induction chemotherapy and chemoradiotherapy in patients with nasopharyngeal carcinoma. J Magn Reson Imaging 2016;43:1179–1190.
22. Ashraf AB, Daye D, Gavenonis S, et al. Identification of intrinsic imaging phenotypes for breast cancer tumors: preliminary associations with gene expression profiles. Radiology 2014;272:374–384.
23. Verhaak RG, Hoadley KA, Purdom E, et al. Integrated genomic analysis identifies clinically relevant subtypes of glioblastoma characterized by abnormalities in PDGFRA, IDH1, EGFR, and NF1. Cancer Cell 2010;17:98–110.
24. Zhang F, Chen JY. Breast cancer subtyping from plasma proteins. BMC Med Genomics 2013;6(Suppl 1):S6.
25. Eisenhauer EA, Therasse P, Bogaerts J, et al. New response evaluation criteria in solid tumours: revised RECIST guideline (version 1.1). Eur J Cancer 2009;45:228–247.
26. Lu Y, Jansen JF, Mazaheri Y, Stambuk HE, Koutcher JA, Shukla-Dave A. Extension of the intravoxel incoherent motion model to non-gaussian diffusion in head and neck cancer. J Magn Reson Imaging 2012;36:1088–1096.
27. Schneider CA, Rasband WS, Eliceiri KW. NIH Image to ImageJ: 25 years of image analysis. Nat Methods 2012;9:671–675.
28. Team RDC. R: a language and environment for statistical computing. Vienna, Austria: R Foundation for Statistical Computing. Available at: http://www.R-project.org. Accessed 2013.
29. StataCorp. Stata Statistical Software: Release 14. College Station, TX: StataCorp LP; 2015.
30. Chenevert TL, McKeever PE, Ross BD. Monitoring early response of experimental brain tumors to therapy using diffusion magnetic resonance imaging. Clin Cancer Res 1997;3:1457–1466.
31. Theilmann RJ, Borders R, Trouard TP, et al. Changes in water mobility measured by diffusion MRI predict response of metastatic breast cancer to chemotherapy. Neoplasia 2004;6:831–837.

32. Driessen JP, van Bemmel AJ, van Kempen PM, et al. Correlation of human papillomavirus status with apparent diffusion coefficient of diffusion-weighted MRI in head and neck squamous cell carcinomas. Head Neck 2016;38(Suppl 1):E613–E618.

33. Chawla S, Kim S, Wang S, Poptani H. Diffusion-weighted imaging in head and neck cancers. Future Oncol 2009;5:959–975.

34. Koh DM, Scurr E, Collins D, et al. Predicting response of colorectal hepatic metastasis: value of pretreatment apparent diffusion coefficients. AJR Am J Roentgenol 2007;188:1001–1008.

35. Srinivasan A, Chenevert TL, Dwamena BA, et al. Utility of pretreatment mean apparent diffusion coefficient and apparent diffusion coefficient histograms in prediction of outcome to chemoradiation in head and neck squamous cell carcinoma. J Comput Assist Tomogr 2012;36:131–137.

36. Barbieri S, Donati OF, Froehlich JM, Thoeny HC. Comparison of intravoxel incoherent motion parameters across MR imagers and field strengths: evaluation in upper abdominal organs. Radiology 2016; 279:784–794.